Image-derived input function estimation on a TOF-enabled PET/MR for cerebral blood flow mapping

Mohammad Mehdi Khalighi[1], Timothy W Deller[2],
Audrey Peiwen Fan[3], Praveen K Gulaka[3], Bin Shen[3],
Prachi Singh[3], Jun-Hyung Park[4], Frederick T Chin[3,4]
and Greg Zaharchuk[3,4]

Abstract

^{15}O-H$_2$O PET imaging is an accurate method to measure cerebral blood flow (CBF) but it requires an arterial input function (AIF). Historically, image-derived AIF estimation suffers from low temporal resolution, spill-in, and spill-over problems. Here, we optimized tracer dose on a time-of-flight PET/MR according to the acquisition-specific noise-equivalent count rate curve. An optimized dose of 850 MBq of ^{15}O-H$_2$O was determined, which allowed sufficient counts to reconstruct a short time-frame PET angiogram (PETA) during the arterial phase. This PETA enabled the measurement of the extent of spill-over, while an MR angiogram was used to measure the true arterial volume for AIF estimation. A segment of the high cervical arteries outside the brain was chosen, where the measured spill-in effects were minimal. CBF studies were performed twice with separate [15O]-H$_2$O injections in 10 healthy subjects, yielding values of 88 ± 16, 44 ± 9, and 58 ± 11 mL/min/100 g for gray matter, white matter, and whole brain, with intra-subject CBF differences of $5.0 \pm 4.0\%$, $4.1 \pm 3.3\%$, and $4.5 \pm 3.7\%$, respectively. A third CBF measurement after the administration of 1 g of acetazolamide showed $35 \pm 23\%$, $29 \pm 20\%$, and $33 \pm 22\%$ increase in gray matter, white matter, and whole brain, respectively. Based on these findings, the proposed noninvasive AIF method provides robust CBF measurement with ^{15}O-H$_2$O PET.

Introduction

Quantification of cerebral blood flow (CBF) is important in the assessment of brain disorders such as stroke or Alzheimer's disease.[1] ^{15}O-H$_2$O PET imaging is an accurate method to measure CBF but it requires knowledge of an arterial input function (AIF) into the brain,[2,3] which is usually acquired using arterial blood sampling. Arterial blood sampling is, however, invasive and labor intensive. Also, because the samples are typically taken from the radial artery in the wrist, the delay and dispersion of the tracer as it travels to the brain must be estimated to derive the AIF.[4] Due to these challenges, some studies have used standardized, population-based AIF functions by averaging the AIF curves measured for a group of subjects.[5,6] However, this method has its own limitations, as the AIF curve is specific to an individual, particularly in clinical patients with cerebrovascular disease.

Alternatively, another approach to noninvasively estimate the AIF curve is with an image-derived input

[1]Global Applied Science Lab, GE Healthcare, Menlo Park, CA, USA
[2]PET/MR Engineering, GE Healthcare, Waukesha, WI, USA
[3]Radiology Department, Stanford University, Stanford, CA, USA
[4]Molecular Imaging Program, Stanford University, Stanford, CA, USA

Corresponding author:
Mohammad Mehdi Khalighi, Global Applied Science Lab, GE Healthcare,
333 Ravenswood Ave., Bldg 307, Menlo Park, CA 94025, USA.
Email: mohammad.khalighi@ge.com

function (IDIF) method. Although IDIF method has been successfully used in large arteries such as femoral arteries[7] and the aortic segment of the heart,[8] its application in the brain has been limited due to the small diameter of the carotid and vertebral arteries compared to the spatial resolution of PET devices. This mismatch leads to two artifacts: (1) spill-over (counts from the tracer inside the artery spreading to adjacent voxels) and (2) spill-in (counts from adjacent voxels spilling into the artery). The spill-over artifact results in lower AIF peak and the spill-in artifact elevates the AIF tail; both will cause errors in CBF estimation. One approach to overcome the spill-over artifact is using partial volume correction with prior knowledge of the PET scanner point spread function.[9–14] However, these methods are very sensitive to precise segmentation of the arteries and depend on the accuracy of the scanner point-spread-function (PSF) measurement, such that a few blood samples are still needed for calibration. Several recent studies have used an MR angiogram for segmenting the arteries;[15–19] these studies offer a more robust segmentation of the arteries but are prone to any misregistration between MR and PET images that are typically acquired in separate sessions. Spill-in can be estimated using two-compartment models that attempt to derive intra- and extravascular contributions to the measured AIF, but may be sensitive to noise.

In this study we have presented a new IDIF method on a PET/MR scanner, which addresses both spill-in and spill-over artifacts, and is minimally sensitive to MRA misregistration effects. First, we optimized the tracer dose level to achieve the best PET image quality for ^{15}O-H$_2$O tracer studies on a time-of-flight (TOF) enabled simultaneous PET/MR scanner. Then, to determine the concentration-time curve of the AIF, all counts (including spill-over) were measured in the cervical carotid and vertebral arteries using a PET angiogram, divided by the true arterial volume using MR angiography. The spill-in problem was minimized by the selection of cervical arteries instead of intracerebral arteries and was further accounted for using the activity in the surrounding tissue for accurate CBF estimation.

Material and methods

Optimized dose calculation

To optimize CBF measurement accuracy, a dose activity level that optimizes CBF quantitation using dynamic ^{15}O-H$_2$O PET data must be determined. Too low injection levels produce insufficient number of true counts and overly high injection levels lead to increased

detector dead-time and excess Poisson noise from random counts. The noise-equivalent count rate (NECR) framework[20] is one method for determining the optimal image signal-to-noise (SNR). NECR behavior varies with scanner geometry, patient size, and activity distribution, which changes during dynamic scanning. We utilized the related acquisition-specific NECR (AS-NECR) method[21] to optimize PET image quality for the most critical time point in the dynamic series, the PET frame corresponding to the AIF peak. The model parameters of the AS-NECR method were tuned for a simultaneous TOF-enabled PET/MR system (GE Healthcare, Waukesha, WI)[22] with a NEMA NECR dataset. The AS-NECR analysis was performed in six subjects (3 male, 3 female; age: 30.2 ± 6.7 yrs; weight: 66.4 ± 10.6 kg; height: 1.70 ± 0.12 m), who were injected with ^{15}O-H$_2$O activity levels between 490 MBq and 960 MBq. Each subject was injected and scanned twice during the same imaging session. As described in more detail later, the AIF curve was estimated using dynamic PET and MR angiography images, with data binned into 3 s dynamic frames over the AIF. The PET frame corresponding to peak AIF was determined from the PET dynamic images (TOF-OSEM, 3 iterations, 28 subsets). The peak AIF frame from each dynamic series was processed with AS-NECR methodology to determine the injection level that would have optimized NECR at the point of the AIF peak.

Basic methodology for AIF measurement

The PET/MR scanner used in this study combines the benefits of high sensitivity[23] and TOF capability,[24] which provides sufficient PET image quality with frames as short as a few seconds for ^{15}O-H$_2$O PET imaging. Because of the 25 cm axial field of view of the detector ring, good sensitivity is also obtained for counts within the neck as well as the brain. Using an appropriate time window during the ^{15}O-H$_2$O arrival to the brain, the cervical arteries can be identified and segmented. The scanner records all coincident prompts and their timing information in the list file. For each 1-second interval, a random estimate[25] is subtracted from the total number of prompts. The remaining counts are trues + scatter (T+S). The time interval when the tracer reaches the axial field of view (i.e. the cervical arteries) is evident in a time plot of T+S. Reconstructing PET images over this short time period provides a PET angiogram (PETA). The PETA is a "blurred" version of the MR angiogram due to the low spatial resolution of the PET detector, which includes spill-over from the cervical arteries. To segment the arteries in PETA images, a rough threshold (mean – one standard deviation of PETA counts) is used to estimate the mean

and standard deviation of the background noise and arteries. These statistics were used to calculate the final threshold using a Bayesian method[26] for segmenting the arterial mask.

By choosing an arterial volume-of-interest in the upper neck rather than the brain itself, we minimize the effect of significant spill-in from the brain parenchyma. Any remaining spill-in is estimated by measuring the average activity of tissues immediately outside this arterial mask, which is then subtracted from the total number of counts in the arterial mask. Because the arterial mask is derived from the PET angiogram, it includes the spill-over events, so the tissue immediately outside this arterial mask is not contaminated by spill-over events. After the spill-in has been addressed, we use accurate volume of these arteries from a simultaneous high-resolution MR angiogram to address spill-over, effectively dividing the true number of counts (which are both within and outside the true arteries due to spill-over) by the true volume of the arteries from which they arise, yielding an AIF measurement in Bq/mL. The MRA images are segmented in a similar way to the PETA images with the exception that first, low-frequency shading was calculated and, consequently, removed using a low pass Gaussian filter. After segmenting the arteries from high-resolution MRA images, the MRA mask is multiplied by the arterial mask derived from PET angiogram to retain only those vessels shown in the arterial mask and then the true arterial volume of vessels shown in the arterial mask was measured from high resolution MRA images. To maximize the signal-to-noise ratio of the AIF curve, the MRA protocol covered the maximum vessel segment in the neck area that was in the PET field of view ($\sim$40 mm in Z direction). The concentration of tracer in the arteries (i.e. the AIF) is quantified as the ratio of the total counts (from PETA) divided by the accurate arterial volume (from MRA).

Subject population and experimental methods

The study was performed in compliance with regulations of the local Institutional Review Board (Stanford University, Administrative Panels for the Protection of Human Subjects) and all subjects provided written consent prior to the study. Ten healthy subjects (5 male and 5 female subjects; age: 41.6 ± 10.7 years; weight: 77.1 ± 10.7 kg; height: 1.69 ± 0.09 m) were hand-injected with 974 ± 79 MBq of ^{15}O-H$_2$O. Each subject received three separate ^{15}O-H$_2$O injections separated by about 20 min; the first two were used to measure CBF reproducibility at baseline, while the final dose was given approximately 15 min after intravenous injection of 1 g of acetazolamide (Diamox), which increased brain perfusion as part of a cerebrovascular reserve challenge. CBF maps (based on the corresponding AIF) were measured within the whole brain separately for each injection. T1-weighted, T2-weighted, and MR angiographic (MRA) images were acquired simultaneously for each subject, with the following parameters: GRE with 30 slices, 667 ms repetition time (TR), 15 ms echo time (TE), flip angle 20°, 24×18 cm field of view (FOV), matrix 256×224, slice thickness 5 mm and scan duration of 1:56 min; T2-FLAIR with 30 slices, TR=9500 ms, TE=141 ms, TI=2300 ms, FOV=24×24 cm, matrix 320×224, slice thickness 5 mm and scan time of 2:32 min; non-contrast TOF with 120 slices, TR = 22 ms, TE=2.4 ms, flip angle 15°, FOV= 22×19.4 cm, matrix 512×384, slice thickness 1.2 mm, voxel size of 0.26 cc, and scan duration of 4:03 min. The coverage of the MRA was from the circle of Willis to the mid-cervical region ($\sim$40 mm), and PETA arterial mask was fixed to cover the same region.

The PET list files were unlisted for every second and total true and scatter coincident events were plotted to identify the time period of tracer arrival into the cervical arteries but before entering brain. A reconstruction was then performed between the time of the first counts appearing to when the count rate was at 75% of the peak count rate in order to generate the PETA and visualize the brain arteries; this was typically on the order of several seconds. The volume was co-localized to the MRA, and all masks were limited superiorly at the level of the petrous carotid arteries to avoid spill-in from the brain.

The PET images were dynamically reconstructed with 1 s frames for 30 s; followed by 3 s frames for 30 s, 5 s frames for 1 min; 10 s frames for 2 min and 30 s frames for 4 min after tracer arrival. The reconstruction was done using TOF-OSEM with 3 iterations and 28 subsets. Attenuation correction, scatter correction, random correction, and dead-time correction were used for the PET reconstruction. While the PET arterial mask includes spill-over, the spill-in mask was composed of neck tissue immediately outside the PET arterial mask by dilating and subtracting the PETA mask by 1 cm, to estimate the spill-in artifact. The total arterial PET count was calculated by subtracting the average counts in the spill-in mask from the total counts in the spill-over mask. Finally, the tracer concentration (AIF) was then calculated by dividing the total arterial PET counts (of each time point in the dynamic PET time series) by the arterial volume measured from MRA images.

Gray and white matter were segmented from the T1-weighted and T2-weighted MR images using unsupervised segmentation method[27] and PET tissue time activity curves were calculated for gray matter, white matter, and the whole brain ROI's. Using a

one-compartment kinetic model with the calculated AIF, CBF and distribution volume were measured by minimizing the mean square of the error between the PET observations and model fit using the Nelder–Mead simplex algorithm[28] in MATLAB (Mathworks, Wilmington, MA). No partial volume correction was performed. In addition to testing the 1st and 2nd runs for intra-subject reproducibility, we also examined the CBF change after the acetazolamide challenge. Furthermore, we divided the cohort into the five youngest (31.8 ± 3.6 year old) and five oldest subjects (51.4 ± 1.7 year old) to determine whether we could observe the known reduction in CBF with increasing age. To further evaluate the performance of the proposed method, it was compared with a population based AIF method. A population AIF was calculated using the mean AIF curve of five subjects (each including two baseline scans) obtained with the proposed method, and was then used to calculate the CBF values of the other five subjects baseline scans. Similarly, a population AIF calculated from the mean of baseline scans of the second group was used to calculate the CBF values of the first group. Owing to the lack of blood samples, the peak of the IDIF curve was used to scale the population AIF for each scan.

Statistical analysis

A one-sample t-test was used to test for a mean difference between the two baseline CBF measurements. A two-sample t-test was used to compare the CBF measurement after acetazolamide administration with the mean of the two baseline measurements. All measurements were considered significant at the $p < 0.05$ level.

Results

PET count rates versus time are shown in Figure 1(a). The AS-NECR curves are calculated for one subject over three different time-frames: the frame corresponding to the peak AIF curve, the frame corresponding to the middle of uptake and a later time-frame, are shown in Figure 1(b) to (d), respectively. The peak relative NECR in (b) is very close to a relative activity of 1 (the actual injection level) and as expected, later PET frames do not achieve maximum AS-NECR because activity has decreased due to isotope decay. The optimal injection level was calculated over the 12 datasets from the six subjects. Optimal injection level was determined to be 840 ± 130 MBq (mean $\pm$ standard deviation). Due to the relatively flat nature of the NECR curve near its peak, a standard site protocol of 850 MBq (23 mCi) was deemed sufficient for the rest of the studies.

Figure 2 shows the trues + scatter coincident prompts over time for one subject. The time marked by (a) starts right after the injection and ends when the tracer enters the field of view (i.e. the cervical arteries). The time marked by (b) starts after the tracers enters the brain arteries and ends approximately at the time the tracer begins to enter the brain parenchyma. By performing a PET reconstruction over this time frame (b), a PET angiogram (PETA) shown in Figure 2(c) is obtained. Figure 2(d) shows the 3D
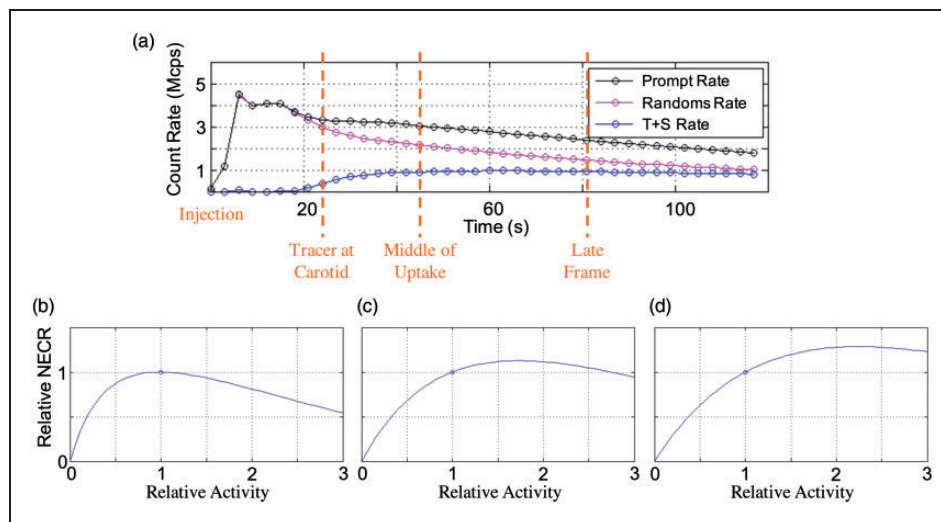

Figure 1. (a) PET count rates versus time. Corresponding AS-NECR curves for three different PET frames: (b) Tracer at carotid, peak AIF; (c) Middle of uptake; (d) Later time frame. This example shows a well-optimized injection level to maximize peak AIF, as the peak relative NECR in (b) is very close to a relative activity of 1 (the actual injection level). As expected, later PET frames do not achieve maximum AS-NECR because activity has decreased due to isotope decay.
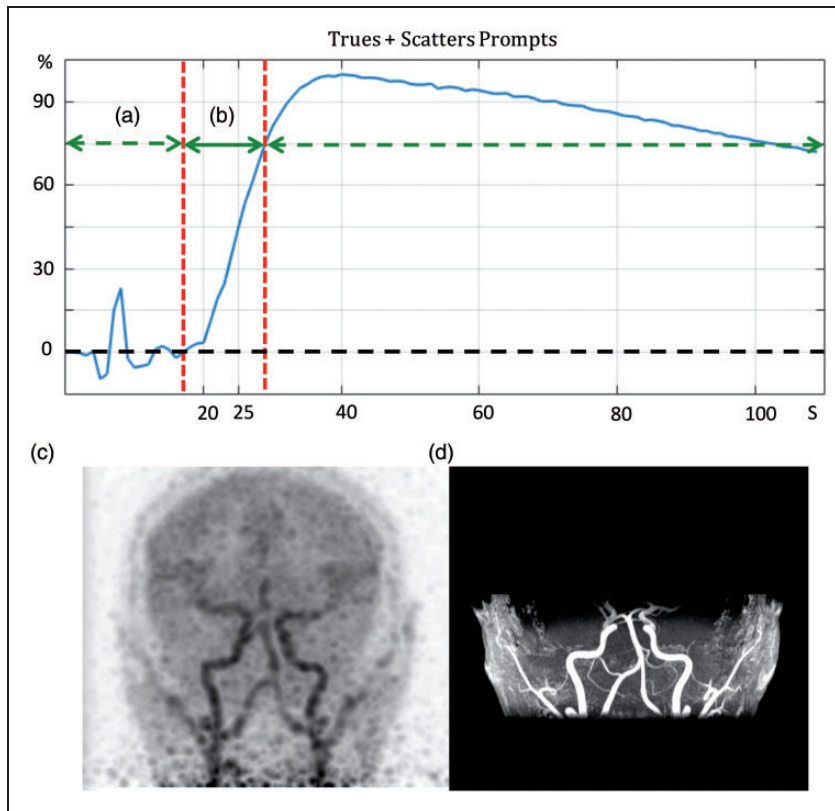
Figure 2. The time interval (a) is from the injection time until the tracer reaches the arterial phase. The time interval (b) is between the arrival of tracer to the point when it enters the brain parenchyma. (c) shows the maximum-intensity projection (MIP) of PET images (coronal view), reconstructed over the 12-second time frame shown in (b), which constitutes a PET angiogram (PETA). (d) shows the coronal MIP of the MR angiogram images acquired simultaneously with the PET acquisition.

MIP (coronal view) of the MRA that was acquired simultaneously for this subject.

Figure 3(a) and (b) shows the 3D MIP (coronal view) of MRA and PETA masks of carotid artery in the neck, respectively. Figure 3(c) shows the extent of the spill-over by overlaying the MRA mask (shown in red) and PETA mask (shown in blue). The mask used to estimate the spill-in is shown in green.

Figure 4 shows the AIF curve estimated by dividing total PET counts within the PETA mask by the arterial volume within the MRA mask and shows that peak AIF occurs at 25 s after the injection. Mean gray matter, white matter, and whole-brain SUV values are also shown. The estimated spill-in activity, calculated from the green mask in Figure 3(c), is also shown.

Figure 5 shows the CBF measurement using AIF estimated by PETA and MRA on 10 different slices of one subject and shows the reproducibility of CBF measurement between the first run (top row) and the second run (bottom row). Figure 6 shows the CBF measurement of one slice per subject before and after acetazolamide injection. Comparison between the top two rows (at baseline) and the bottom row (after the administration of 1 g of acetazolamide) shows the
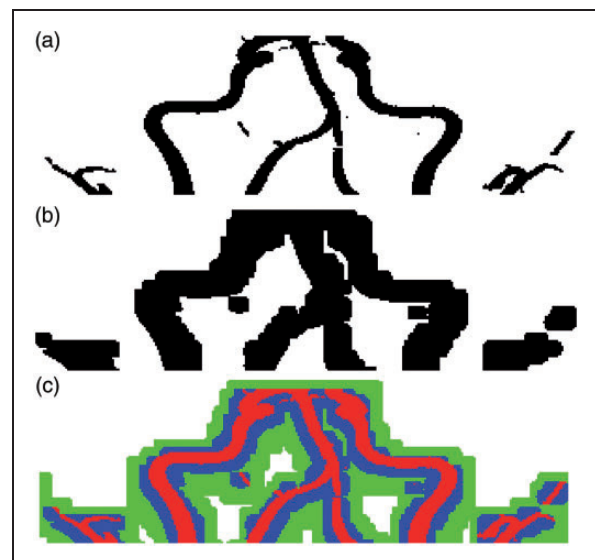

Figure 3. (a) and (b) shows the MRA and PETA masks of carotid artery in the cervical region, respectively. (c) shows the extent of the spill-over by overlaying the MRA mask (shown in red) and PETA mask (shown in blue). The mask used to estimate the spill-in is shown in green.
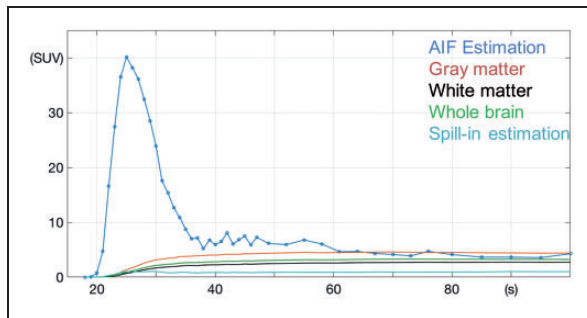
Figure 4. AIF estimated by dividing total PET counts for each time point over the PETA mask by the arterial volume defined by the MRA mask. The average gray matter, white matter, and whole-brain activities are shown. The estimated spill-in activity, calculated by the mask shown in green in Figure 3(c) is also shown.

expected CBF increase due to the acetazolamide challenge. The CBF measurement differences between the 1st run, 2nd run (baseline scans), and 3rd run (after acetazolamide challenge) are summarized in Table 1. Comparison between the 1st and 2nd runs demonstrates a small mean difference of $5.0 \pm 4.0\%$, $4.1 \pm 3.3\%$, and $4.5 \pm 3.7\%$ ($p < 0.03$ for all regions) between the baseline CBF measurements in gray matter, white matter, and whole brain, respectively. The largest difference in CBF measured between the two baseline runs in any individual subject was 13.9%, 10.6%, and 12.0% for gray matter, white matter, and whole brain, respectively.

The mean of all the CBF measurements obtained at baseline was 88.4 ± 16.2, 43.9 ± 9.0, and $58.2 \pm 11.0 \, \text{mL/min/100 g}$ for gray matter, white matter, and
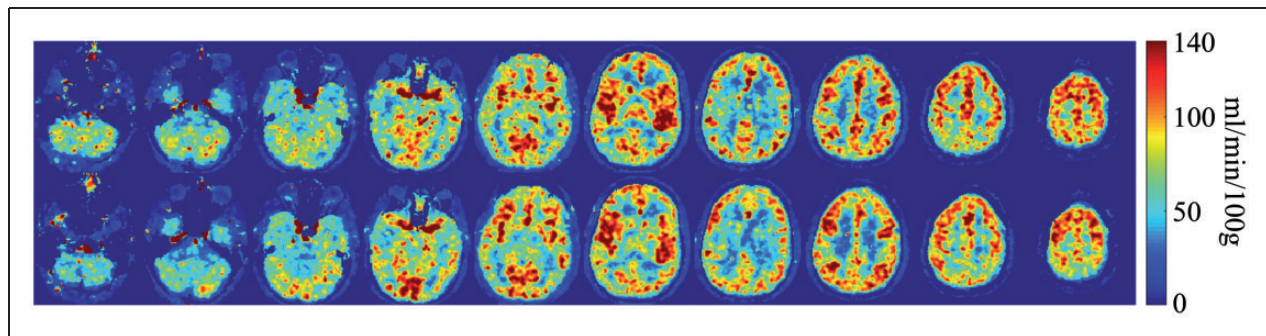

Figure 5. CBF measurement using AIF estimated by PETA and MRA on 10 different slices of one of the subjects. Top row shows the 1st run and bottom row shows the 2nd run CBF measurements.
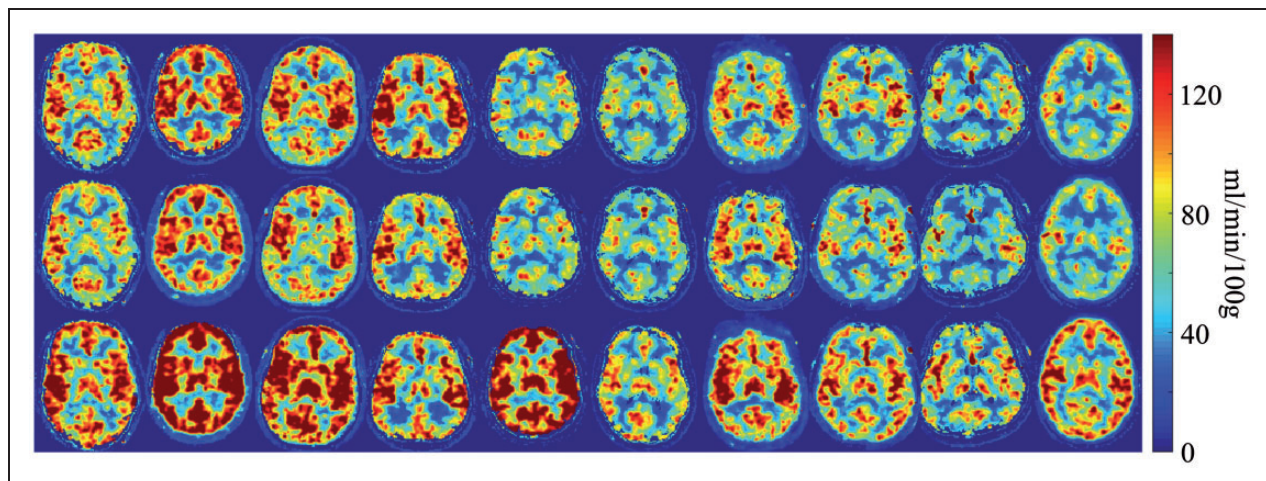

Figure 6. CBF measurement of one slice per subject before and after acetazolamide injection. The top two rows show the CBF measurement of 1st run and 2nd run before acetazolamide administration and the bottom row shows the same measurement after the administration of 1 g of acetazolamide for each subject.

Table 1. Summary of CBF measurements (mL/min/100g) of 10 healthy subjects.

Subjects	Age		Gray matter	White matter	Whole brain
All	41.6 ± 10.7	Run 1	90.2 ± 17.2	44.6 ± 9.4	59.3 ± 11.6
		Run 2	86.6 ± 15.9	43.2 ± 8.9	57.2 ± 11.0
Diff. btw Run 1 and Run 2 (%)			5.0 ± 4.0	4.1 ± 3.3	4.5 ± 3.7
Diff. btw Run 1 and Run 2 (ml/100g/min)			4.4 ± 3.9	1.8 ± 1.5	2.6 ± 2.3
Run 3 (after acetazolamide challenge)			118.8 ± 27.7	56.7 ± 14.2	77.5 ± 18.9
Diff. btw Run 3 and Run 1, 2 (%)			34.9 ± 22.7	29.3 ± 20.3	33.3 ± 21.6
1–5 (younger cohort)	31.8 ± 3.6	Run 1, 2	100.7 ± 12.9	50.9 ± 7.4	67.2 ± 7.7
		Run 3	138.7 ± 23.8	66.7 ± 13.2	91.1 ± 16.5
6–10 (older cohort)	51.4 ± 1.7	Run 1, 2	76.1 ± 7.2	33.6 ± 2.6	44.8 ± 4.4
		Run 3	98.8 ± 12.9	46.7 ± 5.2	63.9 ± 8.4
Diff.	19.6		30.7%	38.1%	37.6%
CBF (mL/100g/min) changes with age (year)		Gray matter	$CBF = 142 - 1.3 \times Age$		
		White matter	$CBF = 74 - 0.7 \times Age$		
		Whole brain	$CBF = 96 - 0.9 \times Age$		

whole brain respectively, which is in line with the previously reported measurements in similar [15O]-PET studies.[29–31] The distribution volume measurements obtained at baseline were 0.99 ± 0.01, 0.68 ± 0.07, and 0.78 ± 0.05 for gray matter, white matter, and whole brain, respectively. The distribution volume measurements obtained after acetazolamide challenge were 0.98 ± 0.06, 0.63 ± 0.06, and 0.74 ± 0.05 for gray matter, white matter, and whole brain, respectively. Because the distribution volumes were similar before and after acetazolamide, we do not expect large scaling errors in the IDIF. Gray-to-white matter ratio was 2.0 ± 0.1, again within literature values for PET. As expected, CBF increased significantly after the administration of acetazolamide, by an average of $34.9 \pm 22.7\%$, $29.3 \pm 20.3\%$, and $33.3 \pm 21.6\%$ in gray matter, white matter, and whole brain, respectively ($p < 0.05$ for all regions). To evaluate the influence of scan time dependency on CBF measures, the baseline CBF (i.e. the first two scans for each patient) was measured using the dynamic PET data for 0 to 1 min, 0 to 2 min, and 0 to 4 min and was compared to measured CBF value using all the dynamic PET data (i.e., 0 to 10 min). The results showed that on average CBF values were $4.9 \pm 1.6\%$, $2.5 \pm 0.9\%$, and $0.8 \pm 0.4\%$ lower using the dynamic PET data for 0 to 1 min, 0 to 2 min, and 0 to 4 min, respectively. This shows that the scan time dependency in the calculated CBF is very small. Comparing the younger and older subjects, who had a mean difference of 19.6 years, we found lower mean CBF in the older subjects ($p < 0.002$ for all regions). Table 1 demonstrates that CBF of the older group is lower by 30.7%, 38.1%, and 37.6% compared to the 19.6-year younger group for gray matter, white matter, and whole brain, respectively.

The difference between the two baseline CBF measurements for each subject using the population AIF is $12 \pm 13\%$, while it was only $4.5 \pm 3.7\%$ for the proposed IDIF method.

Discussion

In this study, we determined the optimal dose for ^{15}O-H_2O CBF measurements using AS-NECR techniques and then developed an automated method to measure the AIF and quantitative CBF from combined PET and MRA information on a simultaneous TOF-enabled PET/MR scanner. Given the need for quantitative CBF measurements, and the difficulty and multiple uncertainties of direct arterial sampling methods, the ability to noninvasively infer the AIF from the images themselves is advantageous. Such a study requires simultaneous acquisition of PET and MR information, to insure the accurate localization of the cervical arterial volume, which can change based on neck position.[32] Furthermore, any assessment of CBF measurements using MRI techniques, such as arterial spin labeling, benefits from the simultaneous acquisition of a reference standard PET map, as CBF is known to change significantly, due to factors such as time of day, caffeine and nicotine consumption, etc.[4]

The total administered radioactivity used by previous ^{15}O-H_2O PET studies ranged between 555 MBq or 15 mCi,[29] and 800 MBq or 21.6 mCi[30] and in one study a larger dose of 1480–1700 MBq or 40–46 mCi[31] is used. In this study, AS-NECR technique was applied to determine optimal injection levels for dynamic PET scanning of the brain. The optimal injection level is specific to the scanner geometry, isotope/tracer, and injection method. An injection protocol of 850 MBq

(23 mCi) was adopted for PET scanning with ^{15}O-H$_2$O for studies on this PET/MR scanner, maximizing AS-NECR at peak AIF. In general, AS-NECR varies based on patient size; however, because the size of the head determines the amount of scatter within the PET field of view and adult head size is sufficiently consistent, it is possible to employ a protocol with fixed activity level for brain. A stronger conclusion could be drawn with a broader range of subject body mass index (BMI) values. In practice, due to the short half-life of ^{15}O-H$_2$O and the numerous steps required for each experiment, the average total administered tracer dose was 974 MBq, which lies in the flat part of the peak AS-NECR curve. Primarily due to its short half-life, effective dose equivalent for ^{15}O-H$_2$O is significantly lower than the equivalent activity injection levels of ^{18}F-FDG.[33,34] Therefore, the activity level selected in this study to maximize NECR has a much lower dose equivalence than a typical FDG injection. By maximizing AS-NECR, we were able to improve the temporal resolution of the PET dynamic frame to 1 s, which is important to capture the peak of the AIF curve in cases with a sharp bolus injection.

In contrast to the current method, previously used methods that employ knowledge of the PET point spread function with the location of the arteries method is highly sensitive to the correct localization of those arteries; historically, co-registered high-resolution MRA images from a separate imaging session have been used to identify the arteries. Because carotid artery position changes based on head position,[35] co-registration of sequentially imaging sessions on two modalities such as PET and MRI is challenging. Simultaneous PET/MR imaging allows for precise segmentation of arteries on the PET image.[15–19] While one study used venous blood sampling to model the residual partial volume effect[16] and another one used fixed assumptions in their model for healthy subjects,[17] all required a priori knowledge of the PSF for the PET detector, which varies across the field of view. Also, these methods are prone to errors due to motion since they rely on precise registration between PET and MR. One advantage of the current technique is that separate methods are used to assess the total number of counts from the arteries and the total volume of the arteries separately, thus minimizing the effects of misregistration between modalities.

In a study comparing eight IDIF methods for dynamic [18F]-FDG PET brain studies,[36] no blood sample free procedure was found to be reliable, suggesting that late venous blood samples should be obtained whenever possible. A review articles on IDIF[37] for brain PET studies has concluded it is a challenging technique that can be successfully implemented in clinical practice only for a small number of tracers and the use of IDIF rarely translates into a less-invasive procedure for the patients, because arterial blood samples cannot be avoided in most cases.

We demonstrated that the carotid and vertebral arteries can be reliably segmented from the PET images automatically, by identifying the arterial phase using the total trues + scatter prompts from all detectors. Spill-out artifact due to the limited resolution of PET detector was measured by a PET arterial mask segmented from a PET angiogram, which was reconstructed from a short time frame (about 15 s) upon arrival of ^{15}O-H$_2$O tracer to the carotid arteries. In order to avoid the spill-in from brain voxels, a segment in the upper neck where the arteries are separated from the high background signal of brain was employed. It should be noted that the carotid artery is the main artery that is used for AIF estimation, which feeds the brain directly; however, it may not reflect the dispersion and delay introduced by abnormalities of the brain arteries, which is a limitation even for the gold standard blood sampling method. Also in the calculation of CBF, the very small delay between the AIF based on the carotid artery and the AIF based on the brain arteries, such as MCA (middle cerebral artery) has been ignored. MRA images were used to measure the arterial volume in order to accurately estimate AIF. It is important to note that precise alignment of the MRA and the PETA is not required for this technique as minor changes in the location due to motion would not impact the measurement of the AIF significantly.

The largest limitation of this study is that we did not perform direct arterial sampling to validate the accuracy of the CBF measurement, as we did not have this capability at our center. However, we were able to measure the precision of the measurement due to the repeated CBF measurements in each participant. We also compared the proposed method with a population-based AIF method, using the average of AIF curves obtained by the proposed method. The population-based AIF resulted in 2.5 times greater difference between the two baseline CBF measurements compared to the proposed method, which highlights the importance of individually measured AIF for each scan.

The attenuation correction provided on the scanner uses an atlas-based algorithm for bone classification in head; however, it is shown[38] that using a more accurate method for bone classification such as zero-TE method[39] results in slightly lower CBF values. One subject out of all 10 subjects showed only 3% increase in CBF after the acetazolamide challenge, while the remaining subjects showed 25–85% increase in CBF with mean value of 37%, which is slightly less than the literature values.[40,41] This may be related to the nonlinear relationship between CBF and the tracer concentration, which may cause larger errors for higher

CBF values. The CBF decrease with age is higher than that reported in Martin et al.,[42] probably due to the lack of partial volume correction. Other limitations include the relatively small patient cohort and the lack of patients with cerebrovascular disease.

Conclusion

Optimal dose and cerebral blood flow measurements were performed using ^{15}O-H_2O PET using an arterial input function measured noninvasively on a PET/MR system. The AIF estimation was reproducible and the measured CBF values were consistent with literature values. The method shows the increased CBF after the administration of acetazolamide and the decreased CBF in older subjects. Based on this, we suggest that it is robust method for measuring CBF, particularly if direct arterial sampling is not possible.

Declaration of conflicting interests

The author(s) declared the following potential conflicts of interest with respect to the research, authorship, and/or publication of this article: Mohammad Mehdi Khalighi and Timothy W Deller are employed by GE Healthcare. Greg Zaharchuk received funding support from GE Healthcare.

Authors' contributions

Mohammad Mehdi Khalighi and Timothy W Deller made a substantial contribution to the design, analysis and interpretation of data. Praveen K Gulaka, Bin Shen, Prachi Singh, Jun-Hyung Park, and Frederick T Chin made a substantial contribution to the concept, design and acquisition of data. Audrey P Fan and Greg Zaharchuk made a substantial contribution to the concept and design, acquisition of data, analysis and interpretation of data. All authors revised the article critically for important intellectual content and approved the version to be published.

References

1. Alsop DC and Detre JB. Perfusion magnetic resonance imaging with continuous arterial spin labeling: Methods and clinical applications in the central nervous system. *Eur J Radiol* 1999; 30: 115–124.

2. Herscovitch P, Markham J and Raichle ME. Brain blood flow measured with intravenous $H_2O(15)$. I. Theory and error analysis. *J Nucl Med* 1983; 24: 782–789.

3. Raichle ME, Martin WR, Herscovitch P, et al. Brain blood flow measured with intravenous H2(15)O. II. Implementation and validation. *J Nucl Med* 1983; 24: 790–798.

4. Fan AP, Jahanian H, Holdsworth SJ, et al. Comparison of cerebral blood flow measurement with 15O-water positron emission tomography and arterial spin labeling magnetic resonance imaging: A systematic review. *J Cereb Blood Flow Metab* 2016; 36: 842–861.

5. Takikawa S, Dhawan V, Spetsieris P, et al. Noninvasive quantitative fluorodeoxyglucose PET studies with an estimated input function derived from a population-based arterial blood curve. *Radiology* 1993; 188: 131–136.

6. Eberl S, Anayat AR, Fulton RR, et al. Evaluation of two population-based input functions for quantitative neurological FDG PET studies. *Eur J Nucl Med* 1997; 24: 299–304.

7. Ludemann L, Sreenivasa G, Michel R, et al. Corrections of arterial input function for dynamic (H2OPET)-O-15 to assess perfusion of pelvic tumours: Arterial blood sampling versus image extraction. *Phys Med Biol* 2006; 51: 2883–2900.

8. van der Weerdt AP, Klein LJ, Boellaard R, et al. Image-derived input functions for determination of MRGlu in cardiac F-18- FDG PET scans. *J Nucl Med* 2001; 42: 1622–1629.

9. Mourik JEM, Lubberink M, Klumpers UMH, et al. Partial volume corrected image derived input functions for dynamic PET brain studies: Methodology and validation for 11C-flumazenil. *Neuroimage* 2008; 39: 1041–1050.

10. Wahl LM, Asselin MC and Nahmias C. Regions of interest in the venous sinuses as input functions for quantitative PET. *J Nucl Med* 1999; 40: 1666–1675.

11. Naganawa M, Kimura Y, Ishii K, et al. Extraction of a plasma time-activity curve from dynamic brain PET images based on independent component analysis. *IEEE Trans Biomed Eng* 2005; 52: 201–210.

12. Fang Y-HD and Muzic RF Jr. Spillover and partial-volume correction for image-derived input functions for small-animal 18F-FDG PET studies. *J Nucl Med* 2008; 49: 606–614.

13. Su Y and Shoghi KI. Single-input-dual-output modeling of image-based input function estimation. *Mol Imag Biol* 2010; 12: 286–294.

14. Simončič U and Zanotti-Fregonara P. Image-derived input function with factor analysis and a-priori information. *Nucl Med Commun* 2015; 36: 187–193.

15. Fung EK and Carson RE. Cerebral blood flow with [15O]water PET studies using an image-derived input function and MR-defined carotid centerlines. *Phys Med Biol* 2013; 58: 1903–1923.

16. da Silva NA, Herzog H, Weirich C, et al. Image-derived input function obtained in a 3TMR-brainPET. *Nucl Instrum Meth Phys Res A* 2013; 702: 22–25.

17. Su Y, Arbelaez AM, Benzinger TLS, et al. Noninvasive estimation of the arterial input function in positron

emission tomography imaging of cerebral blood flow. *J Cereb Blood Flow Metab* 2013; 33: 115–121.

18. Jochimsen TH, Zeisig V, Schulz J, et al. Fully automated calculation of image-derived input function in simultaneous PET/MRI in a sheep model. *EJNMMI Phys* 2016; 3: 2.

19. Sari H, Erlandsson K, Law I, et al. Estimation of an image derived input function with MR-defined carotid arteries in FDG-PET human studies using a novel partial volume correction method. *J Cereb Blood Flow Metab*. Epub ahead of print 24 June 2016. DOI: 10.1177/0271678X16656197.

20. Strother SC, Casey ME and Hoffman EJ. Measuring PET scanner sensitivity: Relating count rates to image signal-to-noise ratios using noise equivalents counts. *IEEE TNS* 1990; 37: 783–788.

21. Stearns CW. Estimating an acquisition-specific NEC curve for PET acquisitions. In: *IEEE NSS conference*, Portalnd, OR, USA, 2003, pp. 2578–2580.

22. Levin CS, Maramraju HS, Khalighi MM, et al. Design features and mutual compatibility studies of the time-of-flight PET capable GE SIGNA PET/MR system. *IEEE TMI* 2016; 35: 1907–1914.

23. Grant A, Deller TW, Khalighi MM, et al. NEMA NU 2-2012 performance studies for the SiPM-based ToF-PET component of the GE SIGNA PET/MR system. *Med Phys* 2016; 43: 2334.

24. Minamimoto R, Levin CS, Jamali M, et al. Improvements in PET image quality in time of flight (TOF) simultaneous PET/MRI. *Mol Imag Biol* 2016; 18: 776–781.

25. Casey ME and Hoffman EJ. Quantitation in positron emission tomography: 7. A technique to reduce noise in accidental coincidence measurements and coincidence efficiency calibration. *J Comput Assist Tomogr* 1986; 10: 845–850.

26. Bernardo J and Smith A. *Bayesian theory*. New York: John Wiley & Sons, 1994.

27. Khalighi MM, Soltanian-Zadeh H and Lucas C. Unsupervised MRI segmentation with spatial connectivity. In: *Proceedings of SPIE, Medical Imaging*, San Diego, CA, USA, 2002, pp. 1742–1750.

28. Lagarias JC, Reeds JA, Wright MH, et al. Convergence properties of the Nelder-Mead simplex method in low dimensions. *SIAM J Optim* 1998; 9: 112–147.

29. Zhang K, Herzog H, Mauler J, et al. Comparison of cerebral blood flow acquired by simultaneous [15O]water positron emission tomography and arterial spin labeling magnetic resonance imaging. *J Cereb Blood Flow Metab* 2014; 34: 1373–1380.

30. Heijtel DF, Mutsaerts HJ, Bakker E, et al. Accuracy and precision of pseudo-continuous arterial spin labeling perfusion during baseline and hypercapnia: A head-to-head comparison with (1)(5)O H(2)O positron emission tomography. *NeuroImage* 2014; 92: 182–192.

31. Ye FQ, Berman KF, Ellmore T, et al. H(2)(15)O PET validation of steady-state arterial spin tagging cerebral blood flow measurements in humans. *Magn Reson Med* 2000; 44: 450–456.

32. Lukins DE, Pilati S and Escott EJ. The moving carotid artery: A retrospective review of the retropharyngeal carotid artery and the incidence of positional changes on serial. *Am J Neuroradiol* 2016; 37: 336–341.

33. ICRP. Radiation dose to patients from radiopharmaceuticals (Addendum to ICRP Publication 53). ICRP Publication 80. *Ann ICRP* 1998; 28.

34. Von Schulthess GK. *Molecular Anatomic Imaging: PET/CT, PET/MR and SPECT CT*. 3rd edition, 2016, LWW.

35. Lukins DE, Pilati S and Escott EJ. The moving carotid artery: A retrospective review of the retropharyngeal carotid artery and the incidence of positional changes on serial studies. *Am J Neuroradiol* 2016; 37: 336–341.

36. Zanotti-Fregonara P, Fadaili el M, Maroy R, et al. Comparison of eight methods for the estimation of the image-derived input function in dynamic [(18)F]-FDG PET human brain studies. *J Cereb Blood Flow Metab* 2009; 29: 1825–1835.

37. Zanotti-Fregonara P, Chen K, Liow J, et al. Image-derived input function for brain PET studies: Many challenges and few opportunities. *J Cereb Blood Flow Metab* 2011; 31: 1986–1998.

38. Khalighi MM, Delso G, Gulaka P, et al. PET/MR attenuation correction using zero echo time imaging in 15O-water study. *ISMRM*. 2016, p.874.

39. Wiesinger F, Sacolick LI, Menini A, et al. Zero TE MR bone imaging in the head. *Magn Reson Med* 2016; 75: 107–114.

40. Vorstrup S, Henriksen L and Paulson OB. Effect of acetazolamide on cerebral blood flow and cerebral metabolic rate for oxygen. *J Clin Invest* 1984; 74: 1634–1639.

41. Lassen NA, Friberg L, Kastrup J, et al. Effects of acetazolamide on cerebral blood flow and brain tissue oxygenation. *Postgrad Med J* 1987; 63: 185–187.

42. Martin AJ1, Friston KJ, Colebatch JG, et al. Decreases in regional cerebral blood flow with normal aging. *J Cereb Blood Flow Metab* 1991; 11: 684–689.